



**HAL**  
open science

# Tension, Compression and Shear Fatigue of a Closed Cell Polymer Foam

Dan Zenkert, Magnus Burman

► **To cite this version:**

Dan Zenkert, Magnus Burman. Tension, Compression and Shear Fatigue of a Closed Cell Polymer Foam. *Composites Science and Technology*, 2009, 69 (6), pp.785. 10.1016/j.compscitech.2008.04.017 . hal-00521262

**HAL Id: hal-00521262**

**<https://hal.science/hal-00521262>**

Submitted on 27 Sep 2010

**HAL** is a multi-disciplinary open access archive for the deposit and dissemination of scientific research documents, whether they are published or not. The documents may come from teaching and research institutions in France or abroad, or from public or private research centers.

L'archive ouverte pluridisciplinaire **HAL**, est destinée au dépôt et à la diffusion de documents scientifiques de niveau recherche, publiés ou non, émanant des établissements d'enseignement et de recherche français ou étrangers, des laboratoires publics ou privés.

## Accepted Manuscript

Tension, Compression and Shear Fatigue of a Closed Cell Polymer Foam

Dan Zenkert, Magnus Burman

PII: S0266-3538(08)00132-2  
DOI: [10.1016/j.compscitech.2008.04.017](https://doi.org/10.1016/j.compscitech.2008.04.017)  
Reference: CSTE 4034

To appear in: *Composites Science and Technology*

Received Date: 3 October 2007  
Revised Date: 9 April 2008  
Accepted Date: 9 April 2008



Please cite this article as: Zenkert, D., Burman, M., Tension, Compression and Shear Fatigue of a Closed Cell Polymer Foam, *Composites Science and Technology* (2008), doi: [10.1016/j.compscitech.2008.04.017](https://doi.org/10.1016/j.compscitech.2008.04.017)

This is a PDF file of an unedited manuscript that has been accepted for publication. As a service to our customers we are providing this early version of the manuscript. The manuscript will undergo copyediting, typesetting, and review of the resulting proof before it is published in its final form. Please note that during the production process errors may be discovered which could affect the content, and all legal disclaimers that apply to the journal pertain.

# Tension, Compression and Shear Fatigue of a Closed Cell Polymer Foam

Dan Zenkert<sup>1</sup> and Magnus Burman

Department of Aeronautical and Vehicle Engineering

Kungliga Tekniska Högskolan (KTH), SE – 100 44 Stockholm, Sweden

Keywords: B: Fatigue, A: Sandwich, D: Life prediction

## Abstract

A closed cell foam of Polymetacrylimide (Rohacell) with three different densities is studied. The foam is tested quasistatically in tension, compression and shear. The tensile properties scale very well with the relative density of the foam, but the compression and shear properties do not scale the same way. It is believed to be due to cell edge and cell wall buckling being the dominated deformation mechanism in compression and shear for lower densities that does not occur for higher densities. Fatigue testing is then performed in tension, compression and shear. It is seen that for all load cases and densities, the fatigue life can be plotted using Basquin's law. The results also show that the different failure mechanisms found in the static tests are the same in fatigue. This means that the fatigue life for different load types exhibit different failure mechanisms. This shows not only as a clear difference in the stress levels for fatigue failure, but also on the slope in the fatigue life relation.

## Introduction

Rigid cellular foams are extensively used as a structural core in load carrying sandwich structures. The usage stretches over applications in aerospace, automotive, marine, transportation and infra-structure. There are numerous examples of applications and a few worth noticing here are the new Swedish Navy Corvette Visby, wind-mill blades, and novel

---

<sup>1</sup> Corresponding author, [danz@kth.se](mailto:danz@kth.se), Ph: +46 8 790 64 35, Fax: +46 8 20 78 65

train car structures. In all of these and many other sandwich applications, the core is typically closed cell polymer foam, designed to carry a substantial part of the load. More and more has been focused on the core material recently due to increased demands for material properties and models to use in the design of sandwich structures. Fracture and fatigue of load carrying foam cores remains to a large extent unknown. The reason for this is the inherent structure of foams, constituted of a complicated 3-dimensional network of thin membranes (cell walls), enclosing each cell. At the intersection of cell walls, edges with concentrated mass build up rods or beams. A foam is not just a material, but also a micro-structure – homogeneous continuum or heterogeneous cell structure, depending on the scale of interest.

Not much has been reported on fatigue of foams. A good summary of what has been done can be found in [1]. Some early work was performed by Burman *et al* [2-3], Shenoi *et al* [4], Buene *et al* [5] and Kanny and Mahfuz [6]. Kanny and Mahfuz [7] and Kulkarni *et al* [8] performed fatigue testing of foam core sandwich beams with polymer foam cores. The testing set-up was in all these cases such that the core would be subjected mainly to shear stress and the intention was to find the stress-life curve for shear stress. McCullough *et al* [9] tested aluminium foams in both tension-tension and compression-compression fatigue. Although the results therein are not given in terms of a Basquins' law, it was found that the slope of the S-N curve is considerably lower in the compression-compression fatigue case. Harte *et al* [10] performed fatigue testing of an open and a closed cell aluminium foam with one aim of finding the fatigue limit. Olurin *et al* [11] performed crack propagation measurement on two closed cell aluminium foams. Shipsha *et al* [12,13] used both compact tension (CT) and cracked sandwich beams specimens to measure crack propagation rates in polymer foams. In both cases, it was found that the crack rates were considerably higher than for homogeneous solid materials. By using micro-mechanics Huang and Lin [14] performed the first attempt to model crack propagation in foams and were able to density normalise the data into one single generic relation for all density phenolic foams. Zenkert *et*

al [15] used an initial flaw approach model through which the crack propagation data could be transformed to stress-life curves. The model gave excellent agreement with measured crack propagation data and tension-tension fatigue testing results for two closed cell polymer foams.

The present study is an extension of the work performed in [15], where only tension fatigue was studied. The aim of this paper is to compare fatigue testing data in tension, compression and shear loading. All the tension data presented here are directly reproduced from [15] but needs to be included in order to make proper comparisons.

## **Materials**

The high performance closed cell rigid polymer foam Rohacell WF-grade was used. Rohacell is a polymetacrylimide (PMI) foam with predominantly closed cells, which is a rather brittle foam with a tensile strain to failure of approximately 2-3%. Details on this material can be found in [16]. Three different densities were used; WF51, WF110 and WF200, with nominal densities of 52, 110 and 205 kg/m<sup>3</sup>, respectively.

## **Static properties**

Static properties of the foams used herein were tested in tension, compression and shear. The tension and compression tests were performed using the same specimen geometry as used in the fatigue testing (described below) at a prescribed displacement rate of 1 mm/minute. The static shear properties were obtained from the same four-point bending test as later used in the fatigue testing. In this test, the shear strength can be obtained, though, the complete stress-strain relation can not be acquired. However, by reducing the load-displacement relation from the test to shear stress (transverse load per unit width divided by core thickness) and readjusting the displacement values so that the initial slope equals the known shear modulus we can get the complete curve, at least approximately. Shear tests performed by the core material manufacturer using the standard block shear test according to ASTM-C273 were used for comparison. The reason for using the bend test

primarily is that block shear test, because of its design, often gives a non-conservative value, at least in strain to failure, and for high density foams.

Fig 1 about here

In tension, the material yields, though very little. We have chosen to use the yield stress as the governing parameter rather than the stress at rupture. The yield point in tension has been defined as a standard 0.2% offset stress, a value being very close to the ultimate strength. In subsequent use of this property, we will refer to this as the yield strength in tension. The values of yield strength are also given in Table 1. There are many interpretations of the compressive strength of foams. As seen from Fig.1, the compressive stress-strain relation can be defined by a linear part, followed by a slight non-linear part, a distinct peak followed by a small stress drop and then a so called plateau level. The manufacturers almost always supply this peak stress in the stress-strain relation as the compressive strength. The material also yields in compression and shear. We have chosen the yield points in compression as a 1% offset stress and in shear as the 0.5% offset stress. There is no particular rationale behind this choice except that these points provide good cut-off stress limits for the fatigue results described in the following sections.

Table 1 about here

In [15] the tensile stress-strain relations were normalised with the density and shown to form a generic relation. The density normalisation was performed using

$$\bar{x} = \alpha \bar{\rho}^n \quad (1)$$

where  $\bar{x}$  is some mechanical property of the foam normalised with its value for the fully dense material (bulk property) of which the cell edges and faces are made of, and  $\bar{\rho}$  is the foam density normalised with the bulk density of the material, the latter taken as 1200 kg/m<sup>3</sup>. This scaling works well when having  $n = 1.1$  for properties like elastic modulus and tensile strength. The actual numbers are included in Table 1. In [15] it was shown that other properties, like fracture toughness, also scale similarly well.

Figure 2 about here

Typical stress-strain relations are given in Fig.1. For reasons of discussion these are plotted in two graphs. In Fig.1a the tensile and compression relations are shown together and in Fig.1b the shear relations are shown. By density normalizing according to eq.(1) using  $n = 1.1$ , the tensile stress-strain relations will almost perfectly overlap for all three densities, as seen in Fig.2a. One can also see from Table 1 that both the elastic modulus and the tensile strength have almost the same normalised number for all three densities. However, the shear strength and compressive strength do not appear to scale the same way. This is seen in Figs.2b and c. The lowest density, WF51, has considerably lower strength and stiffness in shear and compression as compared to its tensile values (see Table 1). For WF200 the situation is almost the opposite, at least the compressive strength is higher than its tensile strength. The reason for this is not proven, but can be explained by the following; the cell wall material is the same for all densities. Higher densities have smaller cells and thicker cell edges and cell walls. Following the procedures by Gibson and Ashby [17], it can be identified that for an idealised open cell foam the cell edge buckling stress is proportional to the relative density square ( $\rho_r^{-2}$ ). A similar reasoning for an idealised closed cell foam would give that cell wall buckling is proportional to the relative density cube ( $\rho_r^{-3}$ ). Thus, buckling is most likely the dominating triggering mechanism for failure in compression for the low density foam, but not for higher densities. Shear loading, being a combination of tension and compression, should then exhibit the same principal mechanism. There are some hints to this in the stress-strain relations given in Fig.1 as well. The WF51 material has a clear non-linear relation in compression for strain larger than approximately 0.5%. For WF110 the compressive stress-strain relation starts becoming non-linear at somewhat higher strains, approximately 0.75%, whereas for the WF200 material the non-linearity starts at above 1% strain. This is also seen in Fig.2b. The non-linear part prior to the peak stress is thus most probably due to cell wall and cell edge buckling, at least for the lower densities. The higher densities have a less pronounced non-linear part which is probably due to plastic hinge formation.

## Crack propagation rate and tensile fatigue testing

In [12] crack propagation tests of Rohacell WF51 were performed using a compact tension (CT) specimen. These results were also reported, although with a more complete set of data, in [15].

The crack propagation measurements were fitted using Paris' law

$$\frac{da}{dN} = C\Delta K_I^m \text{ where } da/dN \text{ is given in mm/cycles} \quad (2)$$

where  $da/dN$  is the crack propagation rate,  $\Delta K_I$  is the stress intensity range,  $m$  is the slope of the relation in a log-log scale and  $C$  is a constant. For details on the data reduction, see [12].

The slope of the Paris' law curve was found by using a least square fit to the experimental results. The slope  $m$  was found to be in order of  $m = 13-14$ . An interesting note that was done was that the Paris' law relation could be scaled with relative density by normalising the cyclic stress intensity factor  $\Delta K_I$  with relative density to the power of 1.1, i.e. the same as the tensile static properties.

There are two important conclusions from these test results; first, the crack growth rate is very high with a high Paris' law exponent. Actually, very high Paris law exponents were reported on Aluminium foams [11], as high as up to  $m = 25$ , although the base material of the foam was aluminium which in its bulk form has a Paris law exponent in the order of 2-4. The second is that the crack propagation can be density normalised in the same manner as static tensile data, and a generic Paris' law curve can be obtained for all densities within this class of materials.

The fatigue test procedure in tension was as outlined in [15]. It uses an axi-symmetric dog bone specimen, described in ASTM D1623-78 "Tensile and tensile adhesion properties of rigid cellular plastics" [18]. The specimens were cut from blocks of foam core, bonded between two aluminium cylinders and a waist was milled to the correct shape and size in a lathe. Thus, this testing is done in the thickness direction of the foam material block.

The fatigue tests were performed under a load controlled sinusoidal cycle using a servo hydraulic testing machine. The load ratio used was in all cases  $R = \sigma_{min} / \sigma_{max} = 0.1$  and a testing frequency of 5 Hz. The fatigue life is characterised as the number of cycles to ultimate failure. There were no visual signs of damage in the specimens prior to failure, which occurred abruptly. The stiffness of the specimens exhibited no measurable change up until the final load cycles prior to complete rupture [15].

### **Compression-compression fatigue testing**

The compression-compression fatigue tests were performed using a similar set-up to the tensile fatigue testing. Cylindrical core samples (same type as in the tensile testing) were bonded to aluminium blocks and tested in fatigue at the load ratio  $R = 10$  (the same as in tension but with negative loads) and with a testing frequency of 5 Hz. Dimensions of the specimen are shown in Fig.3a.

Figure 3 about here

Figure 4 about here

A clip-gauge was mounted to the specimen to measure the displacement in each load cycle (see Fig.3b). The test was interrupted when a permanent strain of 2% was reached (1 mm permanent deformation). At such permanent strain it was found that a crush band had formed in the specimen of a thickness of at least one layer of cells. The crush band can be seen in Fig.4a. An enlargement of the cell structure in the crush band is shown in Fig.4b. One can see that in the crush band, the cell are completely compacted to densification, while the surrounding cells are still intact and unbroken. Every specimen was inspected visually to ensure that a crush band had formed once the test was interrupted. This could also be seen when plotting the maximum or minimum displacement of the clip-gauge during the test. At the formation of a crush band there was a sudden drop in displacement as shown in Fig.5. This figure is intentionally plotted with linear axes, rather than logarithmic, so that the displacement changes appear more clearly. Actually, there are two displacements drops,

the first one occurring at approximately  $3 \cdot 10^5$  load cycles. The drop is approximately 0.4 mm, which corresponds quite well to the average cell size of the material. The displacement drop thus indicates that one layer of cells in the specimens is being crushed and compacted. There are clear indications of a second displacement drop some 20000 cycles later, which most probably indicates that an adjacent layer of cell is crushing.

Figure 5 about here

In Fig.5 one can also notice some creep deformations in the specimen. There was more creep in the compression fatigue testing for higher loads and also more pronounced creep for the lowest density (WF51) than for the higher ones.

### **Shear fatigue testing**

A four point bending rig which enables fatigue loading with both positive and negative loads was used in this investigation, as depicted schematically in Fig.6(a). This design allows the supports to rotate around the neutral axis of the beam in order to minimise the stress concentrations near the load introductions. Furthermore the supports are movable in the beam length direction to enable varying settings of  $L_1$  and  $L_2$ . The supports are also covered with rubber pads in order to smooth out the load transfer. The outer load arms are allowed to move horizontally thus preventing any membrane forces to occur. The tests were performed with sandwich beam specimens, all with glass-fibre composite face sheets manufactured from non-crimp fabrics and vinylester resin using a vacuum infusion process. All specimens were 500 mm long, a width equal to the thickness, and tested using the set-up,  $L_1 = 80$  mm and  $L_2 = 440$  mm. For the WF51 configuration a 50 mm thick core was used with approximately 4 mm thick faces, the WF110 configuration had a 25 mm core with 2.4 mm thick faces and the WF200 configuration had a 32 mm thick core with 3 mm thick face. The testing was performed at  $R = 0.1$  at a testing frequency of 2 Hz.

The failures all occurred between an inner and an outer support, i.e. in the region where the transverse shear force is constant. Failure appeared only on side of beam, though randomly

occurring at either the left or the right region. Since crack propagation rates are so high for this type of material, it is almost impossible to visually locate where cracks initiate and therefore the following discussion is based on how the failure appears post-mortem. For a detailed description on the fatigue crack initiation and propagation in beam specimens like the ones used herein, see [2].

Figure 6 about here

The WF200 specimens all failed by the formation of a 45-degree crack in the core, see Fig.6d. This is a typical shear failure mode for this type of specimen and this is what all static failure modes look like.

The WF51 also had a distinct failure mode indicating that failure initiated and propagated along the face/core interface, as seen in Fig.6b. This is seen from the fact that the final core crack running through the thickness of the specimen has a kinking angle from the interface clearly larger than 45 degrees, rather in the order of 70 degrees. This is evidence that there has been an interfacial macro-crack present just prior to final failure, and when loaded in pure shear this is equivalent of a crack subjected to mode II loading. Such a crack should kink into the core with an angle of approximately 70 degrees [19].

The WF110 exhibited a less consistent and less obvious failure mode, some with interface failures and some with 45-degree shear cracks, see Fig.6c.

### **Results of fatigue testing**

The results of the fatigue testing are shown in Figs.7a-c as standard double logarithmic stress-life relations. They are cut off at the yield strengths of the material as taken from the static testing. However, the choice of yield points was taken so that the cut-off stress provided a consistency with the obtained fatigue data.

Figure 7 about here

From the results given in Fig.7 we can conclude several things: The stress-life data can be plotted using a Basquin's law type relation that reads

$$\Delta\sigma = B(N)^{-\beta} \quad (3)$$

This type of relation seems to fit all the experimental results fairly well, despite obvious experimental scatter. If done so, the life expectancy at yield strength is approximately  $10^2$  cycles, or at least in that order of magnitude, i.e. the linear stress-life curve crosses the horizontal cut-off corresponding to the yield strength at 100 cycles to failure.

One can observe that for the lower density foam (WF51) the S-N curve in shear is close to that in compression. This relates well to the static results for which the compression strength is lower than the tensile strength due to the buckling dominated failure mechanism in compression. Since shear is a combination of tension and compression, it is likely that the shear fatigue results should compare well with the fatigue curve in compression.

For the higher densities, however, the situation is different. For WF110, the S-N curve in compression is higher than both the shear and the tensile S-N curves and shear still below the shear fatigue curve, which follows the static results. For WF200, the compressive strength is higher than the tensile strength, and logically we see that the S-N curve in compression is above that in tension, with the shear S-N curve underneath.

The slope of all S-N curves is another interesting feature. In [15] it was concluded that the slope of the Paris' law curve for the material could be translated to the slope of the S-N curve so that the Paris' law slope  $m$  is translated to the slope of the S-N curve through  $\beta = -1/m$ . Actually, by taking the tensile S-N curves in Fig.7 and making a best fit to the test results, it can be seen that  $m$  is around 14-15 ( $\beta = -1/14$  --  $-1/15$ ). In Fig.7  $m = 14$  has been used. By having a look at the individual densities, one can see the following. For WF51 the tensile S-N curve has a slope  $m \approx 14$  whereas the compressive and shear curves have a lower slope (higher  $m$ ) that is closer to 20 (23 in compression and 20 in shear from a best fit). There is some logic to this, although the behaviour is not clear at this moment. The most probable reason is that the failure mechanism is different in tension to that in compression and shear, thus resulting in different slopes. Shear and compression should exhibit the same failure mechanism and seems to have approximately the same slope. In

tensile loading the cell edges and walls will stretch and bend, whereas in compression and shear the dominating deformation mechanism is most likely buckling.

For WF110 the results are a little more difficult to interpret. The tensile S-N curve has the same slope as the other tensile data. In shear, the slope is the same as in tension, but at a lower stress level. It seems therefore likely that the failure mechanism in shear is the same as in tension. The compression fatigue data has the highest stress level and a lower slope with  $m \approx 24$  from curve fitting. This value is almost the same as for WF51 in compression (and shear). The failure mechanism in compression can thus be assumed to be the same as in compression for WF51, i.e. triggered by cell wall buckling.

For WF200 the picture is clearer. All S-N curves have the same slope with  $m \approx 14$ . The tension and shear curves almost overlap. The compression fatigue data has the same slope but at a higher stress value. This indicates that this higher density material exhibits the same principal failure mechanism in all load cases and that buckling of cell edges and cell walls has little influence on the behaviour.

## Discussion

First, let's have a look at the static properties of these foams. In tension, the static stress-strain relations can be density normalized to collapse into one single relation (Fig.2a).

However, the compressive stress-strain curves do not seem to do this at all (Fig.2b). The reason for this is the different failure mechanisms in tension and compression. In tension, the cell edges and walls in the foam undergo plastic strains and rupture. This mechanism is cell size and cell wall/edge thickness independent.

The crack propagation data can also be density normalised using the same normalisation exponent (1.1), as shown in [15]. The tensile S-N curves for all densities can be treated the same way and will then collapse into one single generic S-N curve [15], which is shown in Fig.8a. The same approach was used for another foam, Divinycell H-grade, in [15].

Figure 8 about here

In compression, on the other hand, cell wall buckling is most probably the dominating mechanism of deformation, at least for the lower density foams. For higher density foams, the cell walls are both smaller and thicker, suppressing buckling. This explains why the compression strength is that much lower than the tensile strength for the lower density foam. The normalised fatigue data in compression and shear are shown in Fig.8b and 8c. They do not collapse into one single generic curve. In compression there is no correlation at all with the two lower densities having a different slope than WF200. However, the WF110 and WF200 are pretty close in terms of normalised stress (Fig.8b) but with different slopes. In shear we see that the WF110 and WF200 normalised fatigue life curves have the same slope, but at slightly different magnitudes. The discrepancy could either be some influence from cell wall buckling or simply that the density scaling is different in shear. An open pending question that cannot be answered at this point is how the failure mechanism in shear fatigue loading actually looks and eventually leads to failure for the lower density foams. The face/core interface separates (debonding failure) after a certain number of loading cycles, but why at the interface and what is the local failure mechanism at cell size level? This is a question for future research.

### **Acknowledgements**

The financial support for this investigation has been provided by The Office of Naval Research (ONR) through programme officer Dr. Yapa D.S. Rajapakse (Grant No. N00014-99-1-0316). Röhm GmbH is acknowledged for supplying the materials. Thanks to Anders Beckman and Bo Magnusson for performing the major parts of the testing.

### **References**

- [1] Sharma N, Gibson RF, Ayorinde EO. "Fatigue of foam and honeycomb core composite sandwich structures: A tutorial", *J. Sand. Struct. & Mat.*, 8(4), 2006, 263-319.
- [2] Burman M. and Zenkert D., "Fatigue of Foam Core Sandwich Beams, Part I: Undamaged Specimens", *Int. J. of Fatigue*, 1997; 19(7), 1997: 551-561.

- [3] Burman M. and Zenkert D., "Fatigue of Foam Core Sandwich Beams, Part II: Effect of Initial Damages", *Int. J. of Fatigue*, 1997; 19(7): 563-578.
- [4] Sheno R.A., Clark S.D. and Allen H.G., "Fatigue Behaviour of Polymer Composite Sandwich Beams", *J. Comp. Mat.*, 1995; 29(18): 2423-2445.
- [5] Buene L., Echtermeyer A.T. and Sund O.E., "Fatigue Properties of PVC Foam Core Materials", *Det Norske Veritas Report 91-2049*, 1991.
- [6] Kanny K. and Mahfuz H., "Flexural fatigue characteristics of sandwich structures at different loading rates", *Comp. Struct.*, 2005; 67(4): 403-410.
- [7] Kanny K., Mahfuz H., Carlsson L.A., Thomas T. and Jeelani S., "Dynamic mechanical analyses and flexural fatigue of PVC foams", *Comp. Struct.*, 2002; 58(2): 175-183.
- [8] Kulkarni N., Mahfuz H., Jeelani S. and Carlsson L.A., "Fatigue crack growth and life prediction of foam core sandwich composites under flexural loading", *Comp. Struct.*, 2003; 59(4): 499-505.
- [9] McCullough K.Y.G., Fleck N.A. and Ashby M.F., "The stress-life fatigue behaviour of aluminium alloy foams", *Fat. & Fract. Engng. Mat. & Struct.*, 2000; 23(3): 199-208.
- [10] Harte A.-M., Fleck N.A. and Ashby M.F., "Fatigue Failure of an Open and a Closed Cell Aluminium Alloy Foam", *Acta Mater.*, 1999; 47(8): 2511-2524.
- [11] Olurin O.B., McCullough K.Y.G., Fleck N.A. and Ashby M.F., "Fatigue Crack Propagation in Aluminium Alloy Foams", *Int. J. of Fatigue*, 2001; 23(5) 375-382.
- [12] Shipsha A., Burman M. and Zenkert D., "On Mode I Fatigue Crack Growth in Foam Core Materials for Sandwich Structures", *J. Sand. Struct. & Mat.*, 2000; 2(2): 103-116.
- [13] Shipsha A., Burman M. and Zenkert D., "Interfacial Fatigue Crack Growth in Foam Core Sandwich Structures", *Fat. & Fract. Engng. Mat. & Struct.*, 1999; 22(2): 123-131.
- [14] Huang J.S. and Lin J.Y., "Fatigue of Cellular Materials", *Acta Mater.*, 1996; 44(1): 289-296

- [15] Zenkert D., Shipsha A. and Burman M., "Fatigue of Closed Cell Foams", *J. Sand. Struct. & Mat.*, 2006; 8(6): 517-538.
- [16] *Rohacell WF*, Röhm Degussa-Hüls group, www.roehm.com
- [17] Gibson L.J. and Ashby M.F., *Cellular Solids – Structure and Properties*, 2:nd edition, Cambridge University Press, Cambridge, UK, 1997.
- [18] *Annual Book of the ASTM Standards*, American Society for Testing and Materials, Philadelphia, PA.
- [19] Zenkert D., "Strength of Sandwich Beams with Interface Debondings", *Composite Structures*, Vol 17, 1991, pp 331-350.

### Figure captions

Figure 1 Typical stress-strain relations for WF51, WF110 and WF200 in (a) tension/compression and (b) tension/shear. Tension curves are in thick lines and compression in thin lines.

Figure 2 Density normalized stress relations in (a) tension, (b) compression and (c) shear

Figure 3 (a) Schematic drawing of the test set-up compression fatigue specimen.

Dimension used  $D = 50$  mm,  $d = 30$  mm,  $H = 50$  mm, and  $h = 32$  mm. (b) Photograph of WF51 specimen mounted in the testing machine.

Figure 4 (a) Photograph of compression-compression fatigue testing set-up and (b) typical crush band fracture in compression fatigue.

Figure 5 Maximum and minimum displacement versus number of cycles in a compression-compression test.

Figure 6 (a) Four-point bending rig and fracture of (b) WF51, (c) WF110 and (d) WF200 specimens after shear fatigue.

Figure 7 Fatigue stress-life diagrams for (a) WF51, (b) WF110 and (c) WF200

Figure 8 Density scaled S-N curves for WF51, WF110 and WF200, (a) tension, (b) compression and (c) shear.

## Tables

	<b>WF51</b>	<b>WF110</b>	<b>WF200</b>
$\rho$ [kg/m <sup>3</sup> ]	52 (52)	114 (110)	207 (205)
$E$ [MPa]	75 (75)	185 (180)	395 (350)
$G$ [MPa]	27 (24)	71 (70)	152 (150)
$\hat{\sigma}_{tension}$ [MPa]	1.6 (1.6)	3.5 (3.7)	7.4 (6.8)
$\hat{\sigma}_{yield}^{tension}$ [MPa]	1.51	3.20	6.45
$\hat{\sigma}_{compression}$ [MPa]	0.95 (0.8)	3.3 (3.60)	8.9 (9.0)
$\hat{\sigma}_{yield}^{compression}$ [MPa]	0.90	3.2	8.0
$\hat{\tau}_{shear}$ [MPa]	0.75 (0.8)	2.5 (2.4)	6.0 (5.0)
$\hat{\tau}_{yield}^{shear}$ [MPa]	0.66	2.4	5.8
$\hat{\sigma}_{compression} / \hat{\sigma}_{tension}$	0.50	0.97	1.32
$\hat{\tau}_{shear} / \hat{\sigma}_{tension}$	0.50	0.73	0.77
$E / \bar{\rho}^n$	2370	2550	2760
$G / \bar{\rho}^n$	760	990	1050
$\hat{\sigma}_{tension} / \bar{\rho}^n$	50	51	48
$\hat{\sigma}_{compression} / \bar{\rho}^n$	25	50	63
$\hat{\tau}_{shear} / \bar{\rho}^n$	25	33	35

Table 1 Material data for Rohacell WF51, WF110 and WF200 (manufacturer's data within parenthesis)

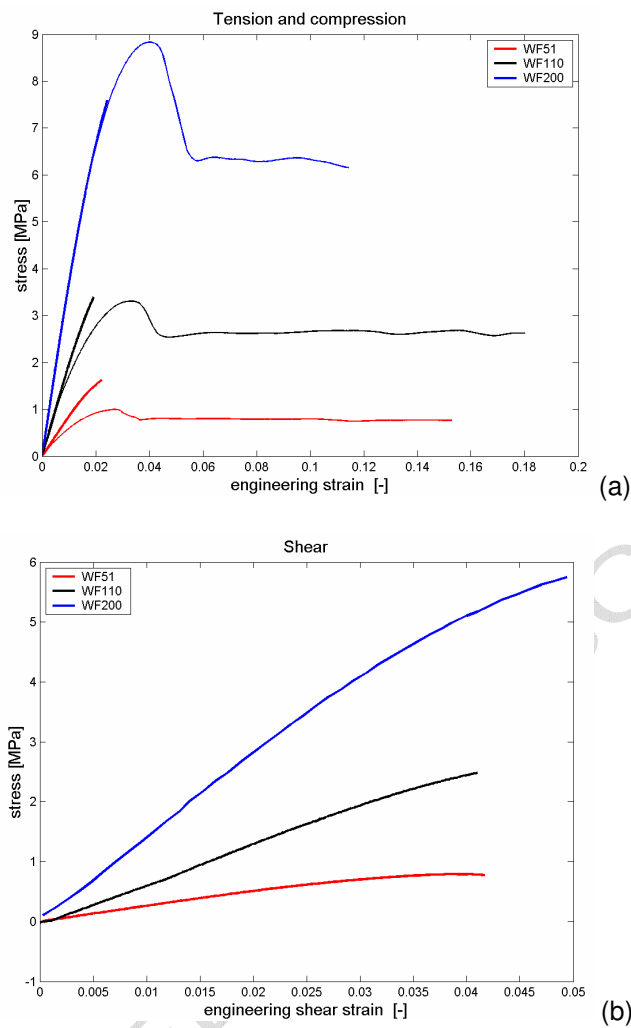


Figure 1 Typical stress-strain relations for WF51, WF110 and WF200 in (a) tension/compression and (b) tension/shear. Tension curves are in thick lines and compression in thin lines.

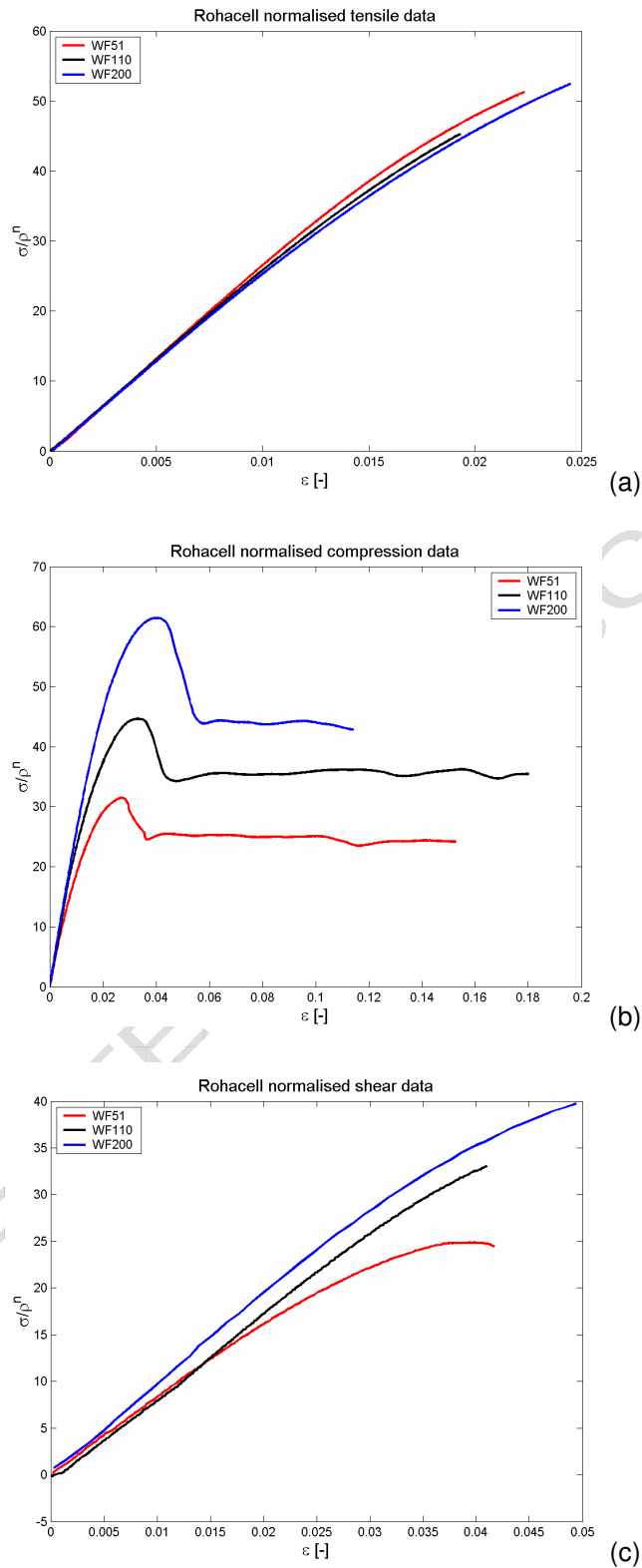


Figure 2 Density normalized stress relations in (a) tension, (b) compression and (c) shear

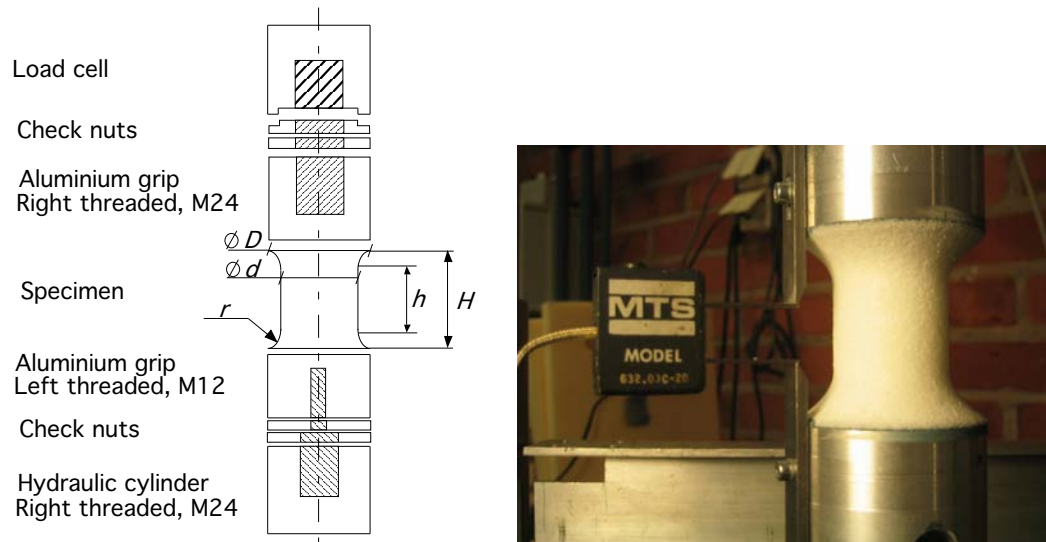


Figure 3 (a) Schematic drawing of the test set-up compression fatigue specimen. Dimension used  $D = 50$  mm,  $d = 30$  mm,  $H = 50$  mm, and  $h = 32$  mm. (b) Photograph of WF51 specimen mounted in the testing machine.

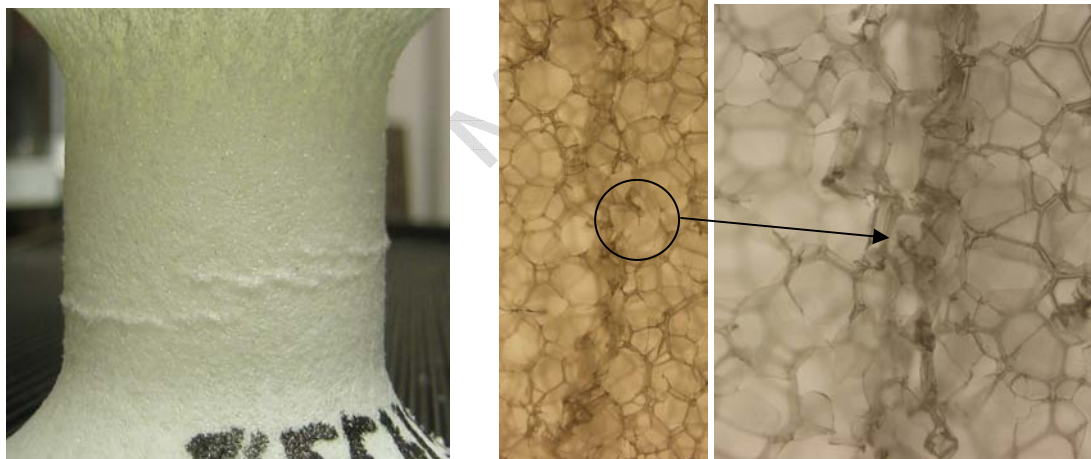


Figure 4 (a) Typical crush band fracture in compression fatigue and (b) micro-graph of the crushed cells in crush-band after failure

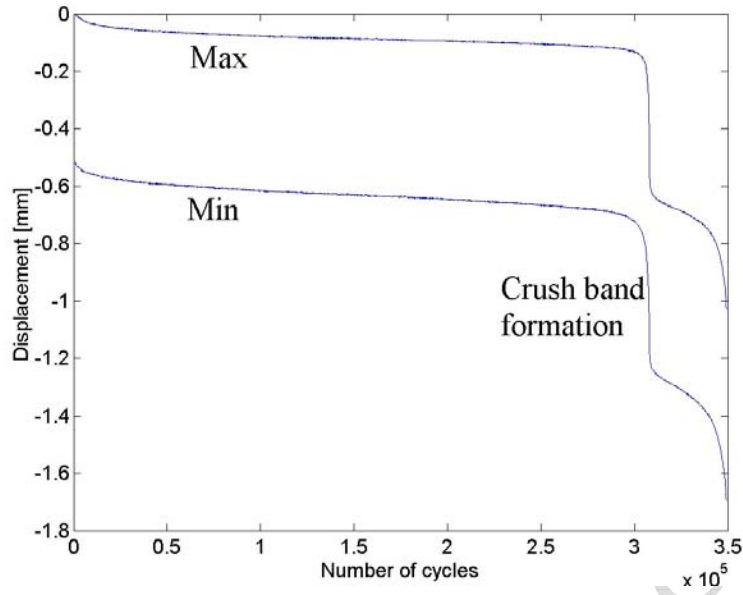


Figure 5 Maximum and minimum displacement versus number of cycles in a compression-compression test.

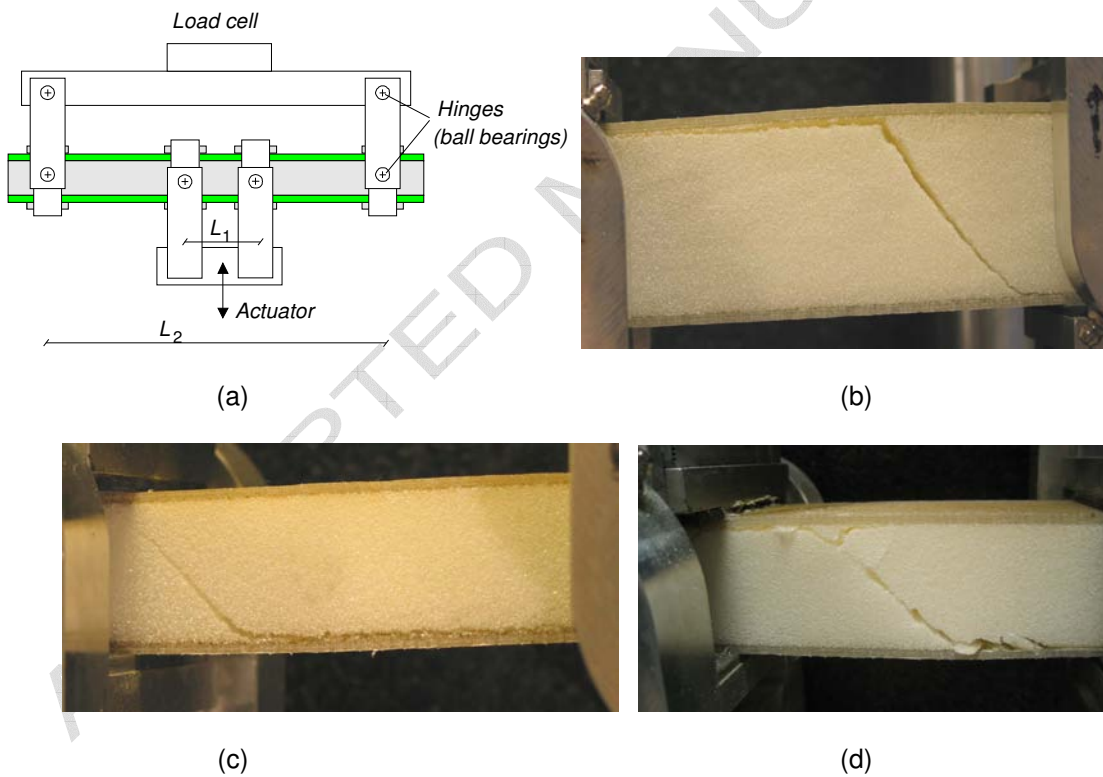


Figure 6 (a) Four-point bending rig and fracture of (b) WF51, (c) WF110 and (d) WF200 specimens after shear fatigue.

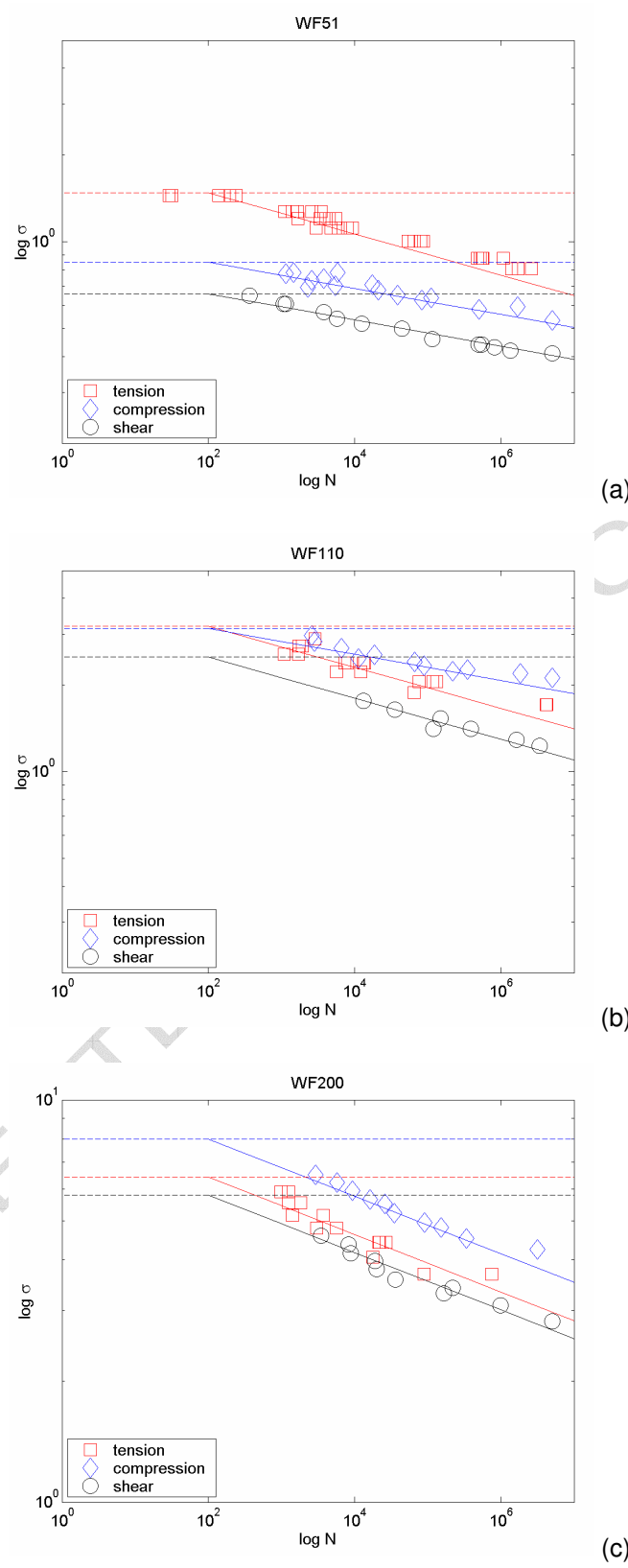


Figure 7 Fatigue stress-life diagrams for (a) WF51, (b) WF110 and (c) WF200

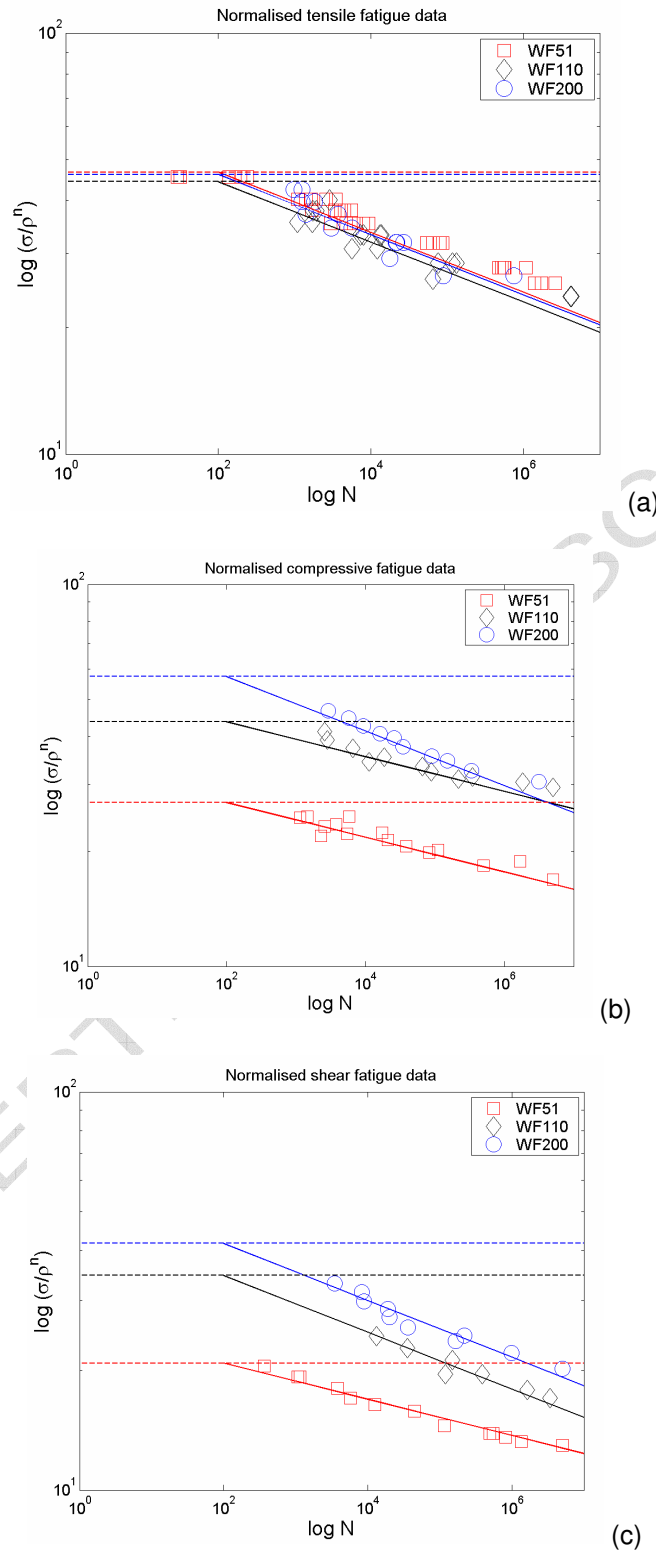


Figure 8 Density scaled S-N curves for WF51, WF110 and WF200, (a) tension, (b) compression and (c) shear.